SPECTRAL CHARACTERISTICS OF THE PEM-EFFECT IN GRADED-GAP $Cd_xHg_{1-x}Te$*

By J. F. Kasprzak, J. M. Pawlikowski, P. Becla and E. Majchrowska

Institute of Physics, Wrocław Technical University**

(Received February 1, 1979; revised version received June 20, 1979)

The spectral characteristics of the photoelectromagnetic (PEM) effect have been measured at 77 and 300 K in the 1–15 μm wavelength range in epitaxial graded-bandgap $Cd_xHg_{1-x}Te$ layers. A simple theory of the PEM-effect in graded-gap semiconductor sample has been presented and the spectral responses of the PEM-effect computed for $Cd_xHg_{1-x}Te$ samples. An adjustment of the theoretical model to the experimental data has been discussed finally.

1. Introduction

The photo-effects in photoconductivity (PC), photovoltaic (PV), and photoelectromagnetic (PEM) modes in a nonhomogeneous semiconductor (e.g. graded band–gap semiconductor with continuity-changed band parameters) are of a great interest because both the effective-mass and energy-gap gradients can strongly influence e.g. the PEM--effect. The first attempt to solve this problem was done by Cohen–Solal and Marfaing in [1] and later works appear in [2–4]. Within these approaches they assumed that the sample is relatively thin hence the carrier excitations take place within the whole sample The position dependence of the carrier-generation rate was also ignored.

A simple theory of the PEM-effect in graded-bandgap semiconductor presented below is based on the Pawlikowski–Kasprzak concept [5] of the "sliced model" of a heterogeneous specimen and will be compared with experimental results obtained from the commonly used method which is extensively described in [6].

---

* This work was supported by the Wrocław Technical University under contract 7/78 (IM-116).

** Address: Instytut Fizyki, Politechnika Wrocławska, Wybrzeże Wyspiańskiego 27, 50-370 Wrocław, Poland.

2. A simple theory of the PEM-effect in graded-bandgap semiconductor[1]

We took the relatively thick graded-gap specimen (with a thickness d) and we assumed that the excess carriers generation process takes place at the same time as the absorption of the monochromatic radiation in a homogeneous, narrow slice with thickness $t(t \ll d)$ in the $X-Y$ plane (see Fig. 1).

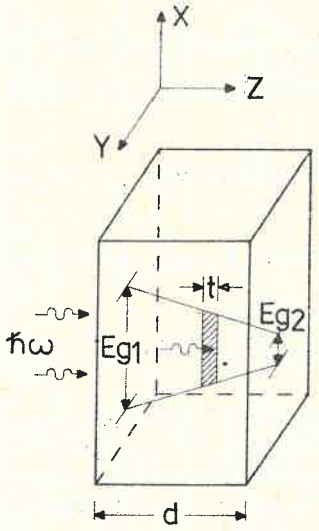

Fig. 1. Outline of graded-gap sample configuration discussed in the text

The thickness t on one hand, corresponds to the width of effective-absorption region in which the falling photon-flux density I_0 decreases e.g. 1000 times and, on the other hand, it is limited by the diffusion length of the minority carriers. For both of these reasons t is of the order of 10–20 μm.

Taking the additional assumptions extensively discussed in [5] and using the continuity equation

$$0 = -\frac{1}{e}\operatorname{div}\vec{j} + G(z) - \frac{p_0\Delta n + n_0\Delta p}{(n_0+p_0)\tau} \tag{1}$$

an the transport equations (according to [7]) we have:

$$\vec{j}_e = e\mu_e n\vec{E}_z + e\mu_e\Delta n\vec{E}_e^G + eD_e \operatorname{grad}\Delta n - \mu_e(\vec{j}_e \times \vec{B}), \tag{2a}$$

$$\vec{j}_h = e\mu_h p\vec{E}_z + e\mu_h\Delta p\vec{E}_h^G - eD_h \operatorname{grad}\Delta p + \mu_h(\vec{j}_h \times \vec{B}), \tag{2b}$$

for electrons and holes, respectively, and in the PEM-effect mode, $\vec{E} = (0, 0, E_z)$ and $\vec{B} = (0, B_y, 0)$, we get for the configuration shown in Fig. 1:

$$j_{ze} = \left[e\left(\frac{1}{n}E_e^G - \frac{1}{p}E_h^G\right)\Delta n + kT\left(\frac{1}{n} + \frac{1}{p}\right)\frac{d(\Delta n)}{dz}\right]\left[(n\mu_e')^{-1} + (p\mu_h')^{-1}\right]^{-1}, \tag{3}$$

[1] This is somewhat better than the results presented in [5].

where $E_z = E_A + E_D$, (E_A and E_D denote the external and Dember field, respectively) μ_e, μ_h, D_e and D_h are the mobilities and diffusion constants for electrons and holes, respectively, $n = n_0 + \Delta n$ and $p = p_0 + \Delta p$ where n_0, p_0, Δn and Δp are the dark and excess concentrations of electrons and holes, respectively, τ is an excess-carriers lifetime, and $\mu'_{e,h} = \mu_{e,h}(1 + \mu^2_{e,h}B^2)^{-1}$. $G(z)$ is the one-dimensional generation rate of photo-carriers and is equal to the rate of photon absorption, i.e., [7]:

$$G(z) = I_0 \exp\left[-\int_0^{z_0} \alpha_0(\xi)d\xi\right]\alpha_m \exp\left[-\int_{z_0}^{z} \alpha_m(\xi)d\xi\right], \tag{4}$$

where I_0 is the rate of incidence of photons per unit front-area of the sample and α_m and α_0 are the maximal and minimal values of absorption coefficient, respectively, [7]. $E^G_{e,h}$ denotes the internal fields existing in graded-bandgap semiconductor [8], having the form as in [1]:

$$E^G_e = \left(\frac{d\varphi_c}{dz} - \frac{3}{2}\frac{1}{e}\frac{kT}{m^*_e}\frac{dm^*_e}{dz}\right), \tag{5a}$$

$$E^G_h = \left(\frac{d\varphi_v}{dz} + \frac{3}{2}\frac{1}{e}\frac{kT}{m^*_h}\frac{dm^*_h}{dz}\right), \tag{5b}$$

where φ_c, φ_v denote the potential of conduction- and valence-band edges, m^*_e and m^*_h are the effective masses of electron and hole, respectively.

Inserting j_{ze} and dj_{ze}/dz into Eq. (1) we obtain the equation which describes the excess-carrier distribution in graded-gap sample (from Fig. 1) in the form:

$$\frac{d^2(\Delta n)}{dz^2} + \frac{W}{P}\left[\frac{d(\Delta n)}{dz}\right]^2 + \frac{U}{P}\frac{d(\Delta n)}{dz}\Delta n + \frac{Q}{P}\frac{d(\Delta n)}{dz} - \frac{R}{P}\frac{\Delta n}{\tau} + \frac{R}{P}G(z) = 0, \tag{6}$$

where

$$W = kT\left[\left(\frac{1}{n^2\mu'_e} + \frac{1}{p^2\mu'_h}\right)\left(\frac{1}{n} + \frac{1}{p}\right) - \left(\frac{1}{n\mu'_e} + \frac{1}{p\mu'_h}\right)\left(\frac{1}{n^2} + \frac{1}{p^2}\right)\right],$$

$$U = \left(\frac{1}{\mu'_h}E^G_e - \frac{1}{\mu'_e}E^G_h\right)\frac{1}{np}\left(\frac{1}{n} - \frac{1}{p}\right),$$

$$Q = e\left(\frac{1}{n}E^G_e - \frac{1}{p}E^G_h\right)\left(\frac{1}{n\mu'_e} + \frac{1}{p\mu'_h}\right),$$

$$R = e\left(\frac{1}{n\mu'_e} + \frac{1}{p\mu'_h}\right)^2, \quad P = kT\left(\frac{1}{n} + \frac{1}{p}\right)\left(\frac{1}{n\mu'_e} + \frac{1}{p\mu'_h}\right).$$

The solution of Eq. (6) is not tabulated, but if we take $W = 0$ which in real cases is true provided that $n_0 = p_0$, i.e., for an intrinsic semiconductor, the following solution is obtained:

$$\Delta n(z) = \Gamma_1 \exp(\gamma_1 z) + \Gamma_2 \exp(\gamma_2 z) + \Gamma_3 \exp(-\alpha_m z) \tag{7}$$

(because, compare [7], $G(z) = I_0\alpha_m \exp(-\alpha_m z)$ in this case) where $\Gamma_{1,2}$ are determined from common boundary conditions [5] and

$$\Gamma_3 = -I_0\alpha_m R\left(\alpha_m^2 P - \alpha_m Q - \frac{R}{\tau}\right)^{-1},$$

$$\gamma_{1,2} = \pm\left[\left(\frac{Q}{2P}\right)^2 + \frac{R}{\tau P}\right]^{1/2} - \frac{Q}{2P}.$$

Taking the literature data of $Cd_xHg_{1-x}Te$ which may be found in [7] and the position dependence of τ in the form

$$\tau = \tau_0 \exp(-a_9 z), \tag{8}$$

where $\tau_0 = 2.2\times10^{-7}$ sec. and $a_9 = 2.5\times10^4\ m^{-1}$, we have obtained the photo-carrier distributions, $\Delta n(z) = \Delta p(z)$, as in [5]. The PEM short-circuit current, PEM-C, can now be obtained by a simple integration

$$\text{PEM}-\text{C} = \sum_{k=1}^{n} w \int_0^{t_k} (j_{xe}+j_{xh})dz = w\sum_{k=1}^{n}(\mu_e+\mu_h)B_y\int_0^{t_k} j_{ze}dz, \tag{9}$$

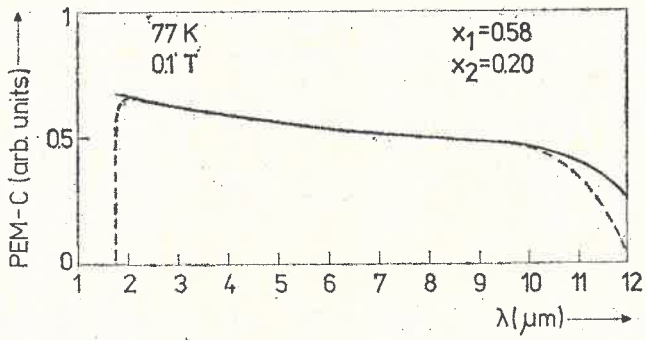

Fig. 2. PEM short-circuit responses of the graded-gap $Cd_xHg_{1-x}Te$ sample computed according to formula (9). Solid line — for surface recombination rates $S_1 = S_2 = 0$ and the broken line — for surface recombination rates $S_1 = S_2 = \infty$. Only excitations by photons with energies $E_{g1} \leqslant \hbar\omega \leqslant E_{g2}$ are included

where w is the width of the specimen and k is a number of the consecutive slice with thickness t. In Fig. 2 the examplary PEM-C responses obtained from Eq. (9) are shown for two different surface recombination rates.

3. Experimental data

In order to compare the experiments with the theoretical model presented above, the PEM-effect in the form of spectral characteristics was extensively measured on graded-gap epitaxial $Cd_xHg_{1-x}Te$ layery. The set-up presented in [6] was used and the measurements were performed at temperatures 77 and 300 K and in the wavelength range

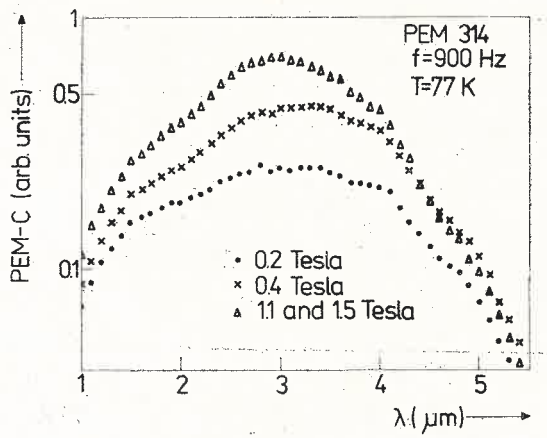

a

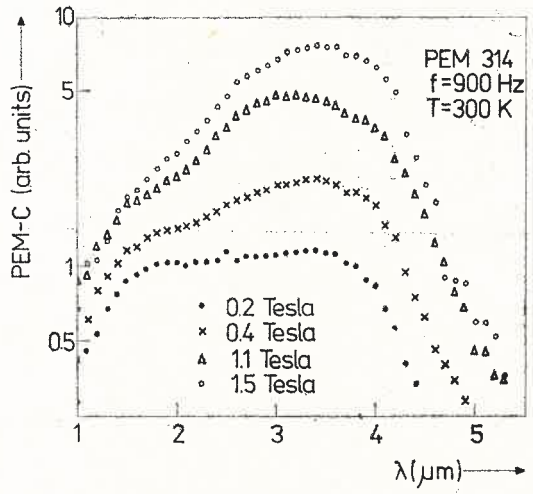

b

Fig. 3. Spectral plots of PEM-C at various magnetic fields of the PEM-314 $Cd_xHg_{1-x}Te$ specimen at 77 K (a) and 300 K (b). Frequency, f, of the chopped light is also marked

of 1–15 μm. Magnetic fields were used in the range of 0.1–2.5 Tesla and radiation was chopped with a frequency in the range of 10–1040 Hz.

Three PEM-response characteristics are shown below as examples of three main types of the samples measured. In Fig. 3, the p-type PEM-314 specimen ($p \cong 10^{23}\mathrm{m}^{-3}$ at 77 K)[2] is presented, with the molar fraction x on both surfaces (see Fig. 1) equal to $x_1 \cong 0.55$ and $x_2 \cong 0.35$ and with a thickness $d \cong 170$ μm. It is the sample type which has low energy-bandgap gradient and a relatively great value of x_2 on the Hg-rich side.

[2] All the values of the carrier concentrations were measured on Hg-rich surfaces of the samples.

It has been noted that the spectral characteristics for low B-values, in fields $B \gtrsim 0.2$ Tesla are flat-topped approximately within the wavelength range of 1.7–3.5 μm, especially at 300 K. We stated that this phenomenon is more apparent in the graded-gap $Cd_xHg_{1-x}Te$ samples than in the homogeneous one in which the PEM-effect was also measured for comparison. The distinct shift in the spectral-plots maximum in high B-values from about 3 μm at 77 K to about 3.5 μm at 300 K is also of interest.

The n-type PEM-318 specimen ($n \cong 10^{22}$ m^{-3} at 77 K) presented in Fig. 4 is an example of the sample which has a high energy-bandgap gradient ($x_1 \cong 1$, $x_2 = 0.28$ and $d = 130$ μm) and the relatively great value of x_2, analogically to the sample PEM-314

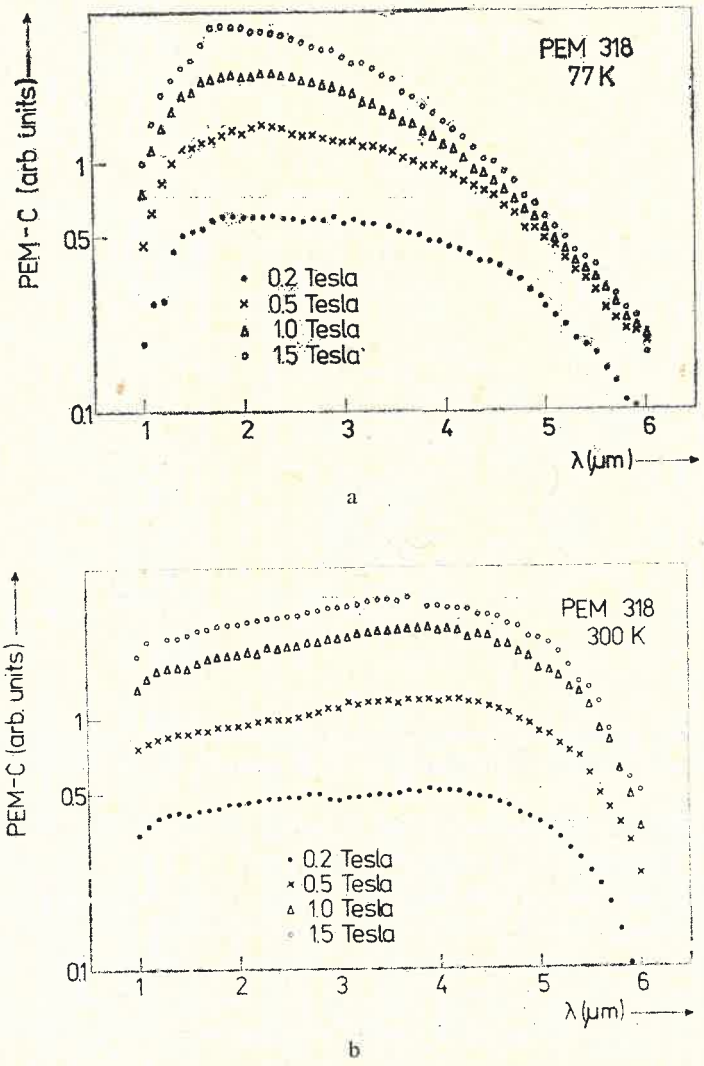

Fig. 4. Spectral plots of PEM-C at various magnetic fields of the PEM-318 $Cd_xHg_{1-x}Te$ specimen at the frequency of the light chopped, $f = 500$ Hz, and at 77 K (a) and 300 K (b)

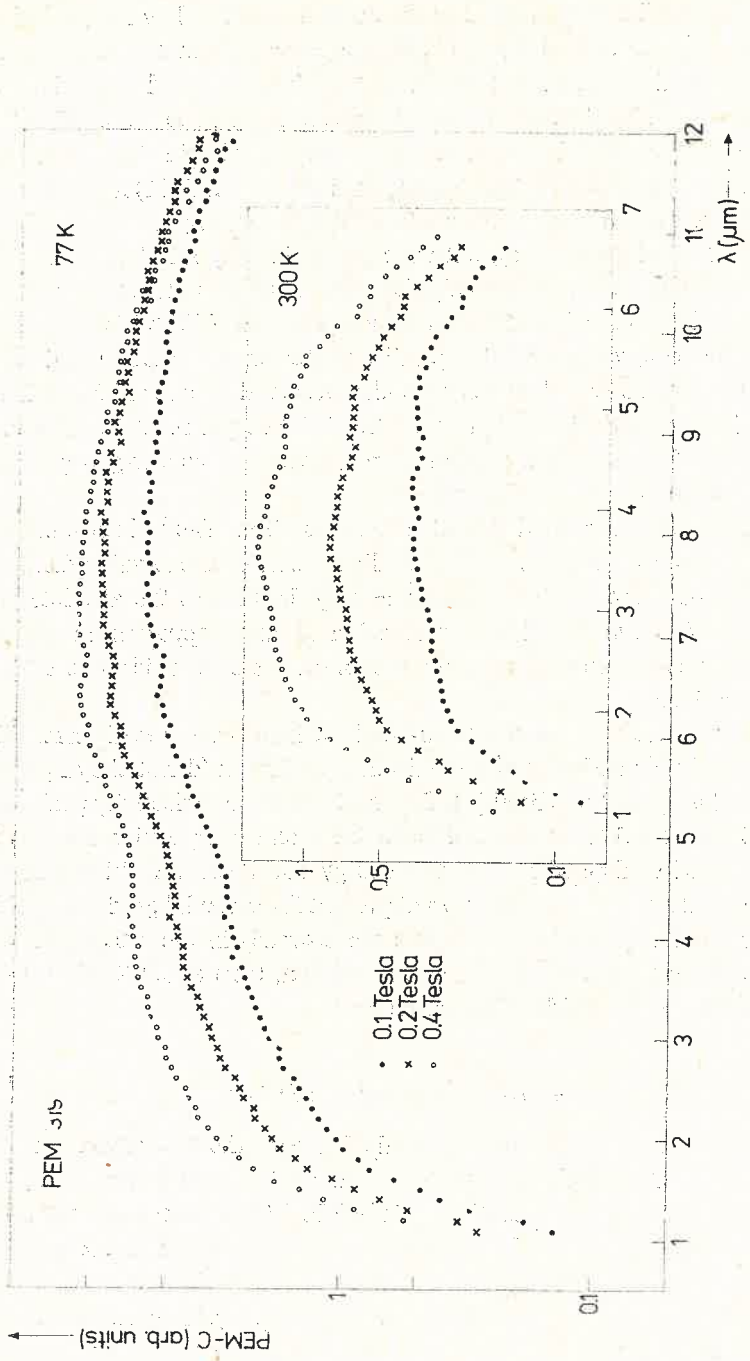

Fig. 5. Spectral plots of PEM-C at various magnetic fields of PEM-319 $Cd_xHg_{1-x}Te$ specimen. Light chopped with a frequency of 10 Hz

presented above. The flat-topped PEM-plots are also found in low magnetic fields and in the wavelength range of about 1.5 μm and 4.5 μm, especially at 300 K. The spectral-plots maximum in the fields at 77 K and 300 K is very dissimilar and located on the λ-scale and shifted distinctly towards the short wavelengths at 77 K. Also we found a displacement of the response peaks at 77 K toward the short wavelengths, in the fields $B > 0.3$ Tesla

In Fig. 5, the p-type PEM-319 specimen ($p \cong 10^{22}$ m^{-3} at 77 K) is given as an example of the third type of sample which has also (see PEM-318) a high energy-bandgap gradient ($x_1 = 1$, $x_2 \cong 0.18$ and $d = 85$ μm), but which has relatively small x_2 values. These small x values locate the energy gap, from the Hg-rich side, of samples close to zero at low temperatures. A new finding is the broader wavelength range at 77 K which is induced by the dependence of the energy-gap of $Cd_xHg_{1-x}Te$ on the molar fraction and temperatures. The steps shown on the spectral curves were also observed in other high-gradient samples. We also noted distinctly higher values of the PEM-response at 77 K than at 300 K, although no regularity, such as dependence on the value of energy-gap gradient or mole fraction, etc., was observed in all samples[3].

Some general remarks should be added to this section. The influence of the magnetic field magnitude is shown in Figs. 3÷5. The diminution of the B-value distinctly flattens the spectral PEM-C response. This simultaneously dimenishes the absolute value of the photo-response. We have stated that this effect is more apparent in the graded-gap $Cd_xHg_{1-x}Te$ specimens than in homogeneous monocrystals in which this effect was measured for comparison.

The molar composition on the front- and back-surfaces was determined from the spectral position of the maximum of the reflection coefficient (denoted by E_1 and $E_1+\Delta E_1$) using the method proposed by Kisiel [9]. This position of the reflectivity peaks corresponds to transitions in the band structure, and hence the molar composition may be determined using the composition dependence of the energy for these transitions. However, this composition dependence is not well known at present for epitaxial graded-gap $Cd_xHg_{1-x}Te$ structures with small x [10]. For this reason the accuracy in the estimation of the molar fraction, x, probably cannot be higher, in our opinion, than about 20% on the back-side and about 5% on the front-side of the specimens.

4. Discussion and conclusions

The first qualitative comparison is made between the theoretical results obtained for homogeneous and graded-gap samples based on the model presented in Section 2. Fig. 6 shows the results of computations of the PEM-C responses of both homogeneous $Cd_xHg_{1-x}Te$ specimens (with mole fraction $x = 0.205$, $x = 0.28$ and $x = 0.55$) and graded-gap sample (with mole fractions on the front- and back-side corresponding to, approximately, the molar composition of homogeneous samples). The surface recombination was not included in computations shown in this figure. Photo-response values of homogeneous samples are plotted in Fig. 6 in the same scale as the computed results. The photo-

[3] However, thermal effects cannot be completely excluded.

response of graded-gap specimen fits in the homogeneous one of $x = 0.55$, for clarification of the figure. The fitting parameter was the density of photon flux, I_0.

It is easy to show that in a homogeneous sample the PEM-C increases with increasing photon energies $\hbar\omega$ beginning approximately from values $\hbar\omega \cong E_g$. In other words, the photoresponse strongly falls down when the decreasing photon energy tends toward E_g

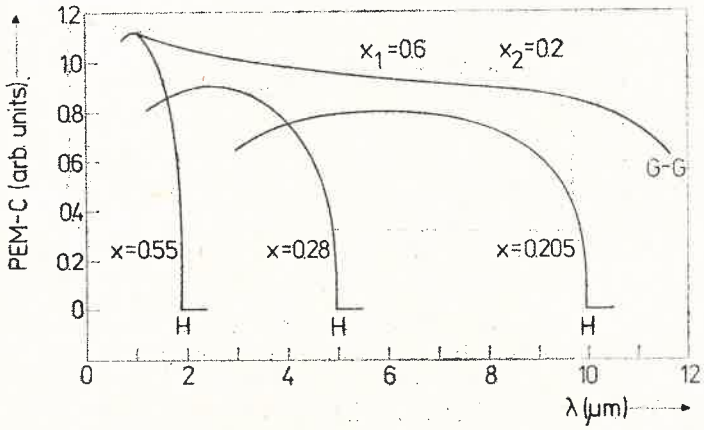

Fig. 6. Theoretical PEM-C plots of both three homogeneous $Cd_xHg_{1-x}Te$ samples (denoted by H) and graded-gap sample (denoted by G-G), at 77 K. The molar compositions are also marked

and later to smaller energy values. In practice, from the higher-energy side, the PEM-C values also strongly decrease due to the surface recombination which is neglected in Fig. 6. Consequently, two main disparities exist between the theoretical PEM-C plots of the homogeneous sample and graded-gap one:

a) The spectral plot of the photoresponse of the graded-gap sample is always broader and covers, in a first approximation, the spectral range lying between the photoresponses of two homogeneous specimens having the mole fractions as the graded-gap sample on its surfaces. This is also true in the photoconductive mode — see [11].

b) The values of the PEM-C spectral plot are greater for graded-gap specimens as a result of the "switching" of consecutive areas of the sample (with changing E_g) to the absorption-generation processes. This was confirmed by us in a simple way. We took, in order to compare with the graded-gap sample, the theoretical "jumped-gap" specimen which was "glued" with some homogeneous samples having molar compositions, x, which changed by 0.05, from sample to sample, and covered the x-range of graded-gap specimen compared The PEM-C spectral curve obtained by, respectively, the addition of the PEM-C response of the all homogeneous samples is always below that of graded-gap specimen (about 10%). The sample dimensions should certainly be the same.

Figure 7 shows an example of a comparison between the experimental PEM-C response of the PEM 318 specimen at a low magnetic field and the theoretical PEM-C plot from Eq. (9) at the same magnetic field and for the appropriate molar composition on both surfaces, including the surface recombination rates, $S_1 = S_2 = \infty$, on both sides.

Two drop-plots in the high-energy region are shown which were obtained from the estimation inaccuracy of both the screening the Debye length and diffusion one which produces an inaccuracy in the estimation of a region of the effective extraction of carriers recombined on the surface states. Nevertheless, a good qualitative coincidence was obtained[4], also in the remaining samples, using only two fitting parameters: the density of photon flux,

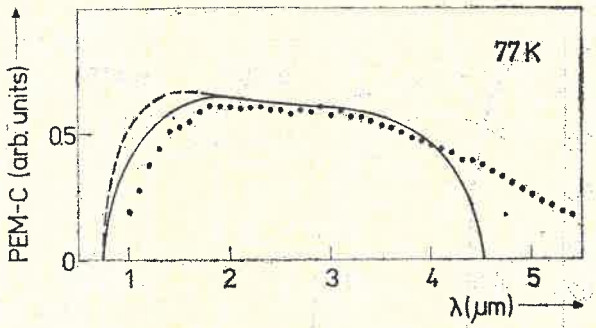

Fig. 7. Comparison between the theoretical PEM-C plot and experimental data of the PEM-318 specimen at 0.2 Tesla. For explanations see text

I_0, which determined only the absolute values of PEM-C responses and the surface recombination rates, $S_{1,2}$, which determined only the rate of the PEM-C decrease on the ends of spectral plots. In practice, both I_0 and $S_{1,2}$ may be changed from sample to sample and, unfortunately, the parameters describing the properties of the inside of specimens, e.g. the mobility, concentration and life-time of the carriers, also may be different than assumed in the model used in the computation procedure.

On the basis of our model two important experimental statements also may be explained.

a) A shift of the maximum of the PEM-C plot, especially in *n*-type specimens, towards a shorter wavelength with an increasing *B*-value is readily understood if we define the meaning of high-mobility carriers ($Cd_xHg_{1-x}Te$ as a semiconductor having extremely mobile electrons, up to $100\ m^2V^{-1}s^{-1}$ at low temperatures, and for $x < 0.2$ [12]). The electron mobility, μ_e, is a function of the mole composition, which at the same time is position dependent in graded-gap $Cd_xHg_{1-x}Te$ specimens. The effect of μ_e on the theoretical PEM-C plot is schematically shown in Fig. 8. The constant excitation (i.e. the total number of excess carriers) in whole graded-gap specimen and $S_1 = S_2 = 0$ are taken to clarify the figure. As is shown, the maximum of the photo-response in the PEM mode is distinctly shifted towards the Cd-rich area with an increasing magnetic field. We neglected the absolute values of PEM-C in this Figure for graded-bandgap $Cd_xHg_{1-x}Te$ specimens.

b) The PEM-C increase with an increasing *B*-value is also easily understood (see Fig. 8). This effect takes place in the Cd-rich area which is confirmed by experimental data.

[4] Certainly, within the limits of estimation errors of a mole fraction and surface recombination rates which, however, may be relatively broad from sample to sample.

In the Hg-rich area the opposite direction of variation is theoretically predicted and this is also in relatively good accordance with the experimental data.

In conclusion we can state that there is a good qualitative agreement found between the theoretical model and the experimental data for the PEM effect in graded-gap $Cd_xHg_{1-x}Te$.

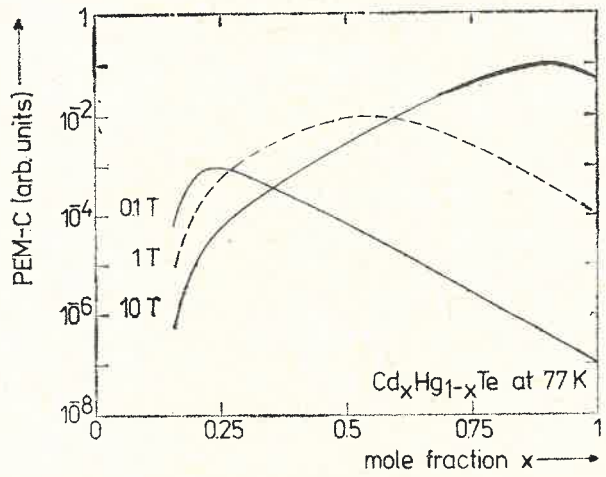

Fig. 8. The shift of the maximum of theoretical PEM-C responses, due to carrier mobility, schematically plotted at various magnetic fields for extremely thin ($t \to 0$) homogeneous slices of graded-gap $Cd_xHg_{1-x}Te$ specimen

In each sample the various $S_{1,2}$, the level excitation and other parameters should be taken into theoretical consideration in order to make a better adjustment.

As was shown, the graded-gap epitaxial $Cd_xHg_{1-x}Te$ layers can be used effectively as relatively broad range infra-red detectors in the PEM mode. Although both the sensitivity and detectivity of the PEM-mode detectors are less than that of the photovoltaic types having *p—n* junctions [13], the first are more broad-ranged being simultaneously easier to produce. It should be also emphasized that they give relatively great values of photo-response at 300 K and do not require any troublesome cooling under the working conditions. However, they require, of course, installing the magnetic field.

REFERENCES

[1] G. Cohen-Solal, Y. Marfaing, *Solid-State Electron.* **11**, 1131 (1968).
[2] S. Sikorski, J. Świderski, *Fotoelektryczne kryteria oceny materiałów półprzewodnikowych*, PWN, Warsaw 1968, p. 56, in Polish.
[3] S. K. Chattopadhyaya, V. K. Mathur, *Phys. Rev.* **B3**, 3390 (1971); **B9**, 3517 (1974).
[4] O. V. Konstantinov, G. V. Tsarenkov, *Fiz. Tekh. Poluprov.* **109**, 720 (1976).
[5] J. M. Pawlikowski, J. F. Kasprzak, *Solid State Commun.* **25**, 645 (1978).
[6] P. Becla, J. F. Kasprzak, J. M. Pawlikowski, *Optica Applicata* **8**, 21 (1978).
[7] J. M. Pawlikowski, *Material Science* **6**, 3 (1980).
[8] H. Kroemer, *RCA Rev.* **18**, 332 (1957).

[9] A. Kisiel, *Acta Phys. Pol.* **A39**, 245 (1971).
[10] A. Kisiel, M. Zimnal-Starnawska, S. A. Ignatowicz, J. M. Pawlikowski, J. Piotrowski, *Thin Solid Films* **37**, L35 (1976).
[11] J. M. Pawlikowski, *Infrared Phys.* **19**, 179 (1979).
[12] J. J. Dubowski, Ph. D. thesis, Wrocław Technical University (1978), unpublished.
[13] P. Becla, J. M. Pawlikowski, *Infrared Phys.* **16**, 457 (1976).